Xiaodong Yu ✉
Zelin Han
Shiwei Zhan
Defan Zhou
Fakun Wang
Fan Sun
Jianhua Jiao
Junfeng Wang
Hui Jiang

https://doi.org/10.21278/TOF.471030321
ISSN 1333-1124
eISSN 1849-1391

MICRO-CLEARANCE OIL FILM TEMPERATURE FIELD CHARACTERISTICS OF HIGH SPEED AND HEAVY TYPE HYDROSTATIC THRUST BEARING UNDER EXTREME OPERATING CONDITIONS

Summary

To explore the micro-clearance oil film temperature field characteristics of hydrostatic thrust bearings under operating conditions of high speed and heavy load, a mathematical model of micro-clearance oil film is established. According to the principle of computational fluid dynamics, the relationship between load capacity and rotational speed is calculated, and the model is solved using the finite volume method. The micro-clearance oil film temperature field is also investigated and tested to verify the theoretical analysis. The results show that the rotational speed is coupled with the load-carrying capacity of hydrostatic thrust bearings. When the extreme operating conditions are between 0t-228.9r/min and 4t-214.9r/min, the oil film maximum temperature increases slowly with the load increase and rotational speed decrease, and the average temperature decreases slowly. On the other hand, when the extreme operating conditions are between 4t-214.9r/min and 32t-78.9r/min, the maximum temperature and the average temperature slowly decrease as the load increases and the rotational speed decreases; the influence of rotational speed is greater than that of load, and the temperature rise of the upstream side is sharper than that of the downstream side.

Key words: *Hydrostatic thrust bearing; Large-scale numerical control equipment; Extreme operating conditions; Micro-clearance oil film temperature field characteristics; Simulation and experimental investigation*

1. Introduction

The hydrostatic thrust bearing has the characteristics of high precision, low power consumption, good vibration absorption performance, long service life, and good stability, and

has become the essential part of large numerical control equipment in the national key industrial fields. With the continuous demand for high speed and heavy duty cutting technologies, the accuracy, size, and speed of machining and the bearing capacity of machine tools are more and more challenging. The performance of micro-clearance oil film has a great influence on the lubrication performance of the hydrostatic thrust bearing; the temperature field of the micro-clearance oil film in particular, affects the deformation of the friction pair of the hydrostatic bearing and the stiffness of the oil film. Therefore, it is very important to study the characteristics of oil film temperature field in the hydrostatic thrust bearing, especially under extreme operating conditions when the temperature of the oil film increases with the increase in the turntable rotational speed and load. The oil film transfers heat to the moving guide rail, deforming the hydrostatic turntable, and the oil film becomes thinner, causing lubrication failure and limiting the improvement in the performance of the hydrostatic turntable. Therefore, it is really necessary to determine the factors that affect the oil film temperature field and determine the distribution law of the oil film temperature field under the condition of high speed and heavy load.

The temperature field characteristics of the micro-clearance oil film of hydrostatic thrust bearings have become one of the main factors affecting the normal operation of the machinery; therefore, they have attracted the attention of many researchers. Heng Fengqin [1] analysed the thermal characteristics of the oil film between the guide rail and the base of the static pressure turntable, and presented the law of the influence of the oil film heating on the thermal deformation of the static pressure turntable. Zhang Yanqin [2-5] studied the heavy load, temperature rise, and high-speed characteristics of micro-bevelled oil pad hydrostatic bearing using the finite volume method. Yu Xiaodong [6] simulated the thermal deformation of the hydrostatic thrust bearing turntable and base using the fluid-structure coupling method, and revealed the thermal deformation distribution. Yu Xiaodong [7] derived the relationship between the rotational speed, load, and the thickness of the clearance oil film of the annular cavity multi-oil cushion hydrostatic thrust bearing rotary table by combining theoretical analysis and experimental verification and designed the experimental setup of oil film thickness. Fathimunnisa Begum [8] carried out tribological experiments with jatropha biofluid and nanoparticles used as lubricant additives. Ma Tao [9] applied the computational fluid dynamics software FLUENT to discuss the pressure field and temperature field of the liquid hybrid bearing; in the results, he obtained the pressure and temperature field distribution of the hybrid bearing, and revealed the influence of the eccentricity on the load carrying capacity. Wang Junyao [10] obtained the heating performance of an embossing-head by using electromagnetic induction heating. Zhang Jingdong [11] simulated the temperature field and pressure field of the oil film in the gap of the hydrostatic rotary table using the fluid mechanics calculation software FLUENT, and investigated the influence of the speed of the rotary table and the depth of the oil cavity on the oil film temperature and pressure fields. Nikola Vujnović [12] pointed out the differences in calculations of annual heating and cooling energy by modifying the simple hourly method and by using dynamic simulations. Fang Long [13] solved unsteady mass, momentum and heat equations of oil film by using Matlab, and provided a theoretical method to analyse the flow and heat transfer characteristics of oil film in hydrostatic thrust bearings. Šefik Behrem [14] presented the heat transfer coefficient estimation during the quenching of cylindrical samples in aqueous solutions. Shao Junpeng [15] adopted the finite volume method to simulate the temperature field of the fluid between the fan-shaped cavity and the circular cavity, and established the governing equation in the rotating coordinate system; he discussed the temperature field of the two cavity shapes at the same speed, cavity depth, and effective bearing area, and optimized the structure of the oil cavity. Lang Ji [16] put forward a coupling analysis model for thermal effects of sliding bearings, and coupled and solved mass, momentum, energy, and physical property equations. Liu Daquan [17] established a one-

dimensional temperature field calculation model for sliding bearings based on the two-dimensional temperature field model and obtained the thermal boundary conditions of the contact surface of the bearing pad, the control equations of the circumferential one-dimensional oil film temperature field, and the analytical expression of the inner surface temperature of the bearing pad. Zhang Guotao [18] established a thermo-hydrodynamic lubrication model for a circular double-layer porous bearing in combination with fluid pressure and heat transfer equations, and revealed the basic source of heat generation and its transfer mechanism. Brito F P [19] presented an experimental and theoretical study on the thermal behaviour of metallic elliptical and offset-halves journal-bearing configurations of the same geometrical size under low-to-high operating conditions using three different commercially available grades of oils. Singh U [20] performed a theoretical, steady-state thermo-hydrodynamic analysis of an axial groove journal bearing in which oil was supplied at constant pressure.

At present, the research on the 3D temperature field is not perfect at home in China and abroad, and there is a lack of direct methods for measuring the micro-clearance oil film temperature field. Therefore, a three-dimensional finite element model of micro-clearance oil film has been established, and the temperature field distribution characteristics of the micro-clearance oil film of the hydrostatic thrust bearing under extreme operating conditions of high speed and heavy load have been determined. It is of great practical significance to better control the oil film temperature and reduce the thermal deformation of the hydrostatic thrust bearing.

2. Relationship between load capacity and rotational speed under extreme operating conditions

Extreme operating conditions refer to the operating conditions in which the maximum rotational speed can be achieved at a certain load, or the operating conditions in which the maximum load can be achieved at a certain rotational speed.

2.1 Working principle of hydrostatic thrust bearings

Constant flow hydrostatic thrust bearings are used to supply oil by means of a quantitative oil pump; the oil is delivered to the hydrostatic oil chamber of the thrust bearing through the oil separator. Since the lubricating oil has pressure, a lubricating oil layer is formed in the oil chamber, and the bearing capacity of hydrostatic thrust bearings is produced using the pressure difference between the hydrostatic oil chambers, and lubricants can float the thrust bearing turntable and withstand external loads [21-24]. The working principle of a constant flow hydrostatic thrust bearing is shown in Fig. 1.

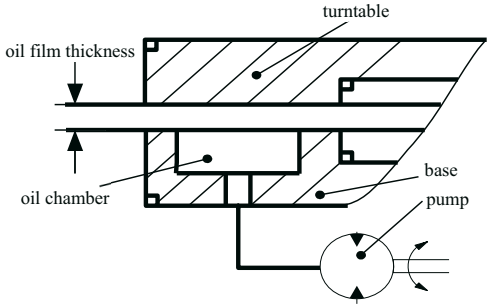

Fig. 1 Working principle of a constant flow hydrostatic thrust bearing

2.2 Inertia flow rate of double rectangular chamber

Due to the rotation of the turntable, the lubricating oil in the double rectangular oil chamber is thrown out and the pressure in the oil chamber drops. The flow rate in the oil

chamber under the centrifugal force can be obtained by substituting the boundary conditions. The inertia flow rate in the single rectangular chamber is shown in equation (1).

$$Q_\omega = \int_0^h \frac{\rho r\omega^2}{12\mu} 2\pi rhy\left(1-\frac{y^3}{h^3}\right)\mathrm{d}y = \frac{\pi}{20\mu}\rho h^3\omega^2 r^2, \tag{1}$$

where μ is the kinematic viscosity, ρ is the lubricating oil density, w is the angular velocity, h is the oil film thickness, and r is the turning radius.

The area ratio K of the double rectangular chamber to the circular chamber is shown in equation (2).

$$K = \frac{24\times A_e}{\pi\left(R_1^2 - R_3^2\right)} \tag{2}$$

where K is the area ratio, and R_1 and R_3 are the inside and the outside radius of the circular chamber.

The amount of oil leakage of the oil pad in the double rectangular chamber is shown in equation (3).

$$Q_\omega = K\left(\int_{R_3}^{R_1}\frac{\pi}{20\mu}\rho h^3\omega^2 r^2 d_r - \frac{\pi}{20\mu}\rho h^3\omega^2 R_3\right) \tag{3}$$

2.3 Relationship between load capacity and rotational speed

With the high-speed operation of the turntable, part of the hydraulic oil is discharged from the oil chamber due to the centrifugal force, resulting in a decrease in the film thickness; as the rotational speed increases, the film thickness decreases more rapidly. When the oil film thickness drops to 0.04 mm, a machine alarm is activated. If the safety factor is 1.5, the calculated film thickness is not less than 0.06 mm. The inertia flow rate caused the film thickness to decrease; the relationship between the inertia flow rate and the oil film thickness is shown in equation (4).

$$\frac{h}{h_\omega} = \frac{\sqrt[3]{\dfrac{3Q\mu}{P_1\left(\dfrac{l}{B-b}+\dfrac{b}{L-l}\right)}}}{\sqrt[3]{\dfrac{3Q_\omega\mu}{P_1\left(\dfrac{l}{B-b}+\dfrac{b}{L-l}\right)}}} = \sqrt[3]{\frac{Q}{Q_\omega}}, \tag{4}$$

where Q is the total flow rate, B, b, L, and l are the outside and the inside width, the outside and the inside length of single rectangular oil chamber, and h_ω is the oil film thickness corresponding to the inertia flow rate.

The ejection of hydraulic oil results in a decrease in the film thickness. Under the same load, different oil film thicknesses require different flow rates. Therefore, the difference between the flow rate of 0.1 mm and 0.06 mm of oil film thickness is the amount of oil leakage at this time.

$$\omega = \sqrt{\frac{20Q\left(1-\frac{h_\omega^3}{h^3}\right)\mu}{\pi K h_\omega^3 \rho\left(\frac{R_1^3-R_3^3}{3}-R_3^2\right)}} \tag{5}$$

The relationship between rotational speed and load under extreme conditions can be obtained from equation (5), as shown in Table 1.

Table 1 Relationship between rotational speed and load under extreme conditions

Load(t)	0	4	8	12	16	20	24	28	32
Rotational speed (r/min)	228.9	214.9	196.7	182.3	162.4	147.2	127.1	108.4	78.9

2.4 Oil film temperature rise

When the hydrostatic turntable is rotating, the temperature of the hydraulic oil gradually increases. Generally, to ensure proper operation, the hydraulic oil needs to be cooled. The main causes of hydraulic oil temperature rise are friction power consumption and pump power consumption. Firstly, there is a relative motion of hydraulic oil between the turntable and the base. The shearing of the oil film will consume the power of the motor, and this part of the shear force will eventually be converted into heat to increase the temperature of the oil film. The friction power consumption is calculated according to equation (6).

$$N_f = \sum \mu A_f \frac{v^2}{h_0}, \tag{6}$$

where N_f is the friction power consumption, A_f is the friction area, h_0 is the initial oil film thickness, and v is the linear velocity.

From equation (6) one can see that the friction power consumption is only related to the relative rotational speed when determining the shape of the oil chamber, the type of hydraulic oil, and the load. In the entire area of the oil chamber, the sum of velocity vectors is always equal to the rotational speed of the turntable.

In addition, under certain operating conditions, the hydrostatic turntable is lost by the throttle, support clearance, pipeline valves and filters, and the power consumed is called the output power of the pump. Since the pressure drops to zero after the hydraulic oil flows out of the hydrostatic support oil chamber, the input power of the system oil pump has been completely consumed; the flow rate of the relief valve of the oil pump is shown in equation (7).

$$Q_p = K_q \sum Q, \tag{7}$$

where Q_p is the oil pump flow rate and K_q is the flow coefficient.

The total power consumption of the pump is calculated based on the initial state of the flow, as shown in equation (8).

$$N_p = \frac{p_s Q_p}{102 \times 100} \approx p_s Q_p \times 10^{-4}, \tag{8}$$

where p_s is the supply oil pressure.

It is assumed that the temperature rise of the lubricating oil is caused by the heat generated by the total power consumption, as shown in equation (9).

$$\Delta t = \frac{1}{JC_0\rho Q}\left(p_s Q \times 10^{-4} + \mu\omega^2 r^2 \frac{A_f}{h} \times 10^{-4} \right), \tag{9}$$

where Δt is the temperature rise, C_0 is the specific heat capacity, and J is the mechanical equivalent of heat.

3. Model and meshing of micro-clearance oil film

3.1 Micro-clearance oil film model

The liquid in a hydrostatic turntable is a laminar flow. When the hydrostatic turntable is stable, an oil film will be formed between the turntable and the oil pad. In order to reduce the amount of calculation, an oil pad is selected as the research object and the three-dimensional structure of the oil film was established by Unigraphics (UG), as shown in Fig. 2. The corresponding oil film models under different loads are established, respectively.

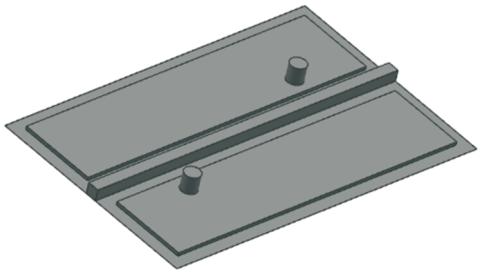

Fig. 2 Micro-clearance oil film model

3.2 Micro-clearance oil film mesh

A three dimensional geometry model of the oil film is established by UG, and is imported into the ICEM CFD to generate grid. The micro-clearance oil film model is shown in Fig. 3.A structural hexahedron grid is used for the complex geometry oil film; this grid inherits the advantage of the Cartesian grid and an unstructured grid, and it may save the quantity and enhance the quality of the grid [25-27]. The total number of the grid is 1006354, and the quality distribution below 0.8 is 0; the grid number between 0.8-0.9 is 7568, which accounts for a total of 0.75%, while the grid number between 0.9-1.0 is 998786, which accounts for a total of 99.25%. The micro-clearance oil film grid model block map is shown in Fig. 4, and the grid quality is shown in Fig. 5.

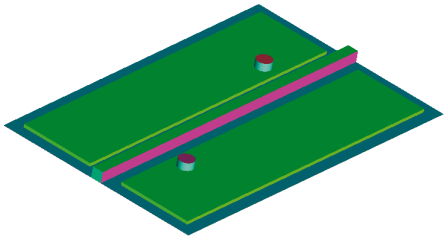

Fig. 3 Micro-clearance oil film grid model

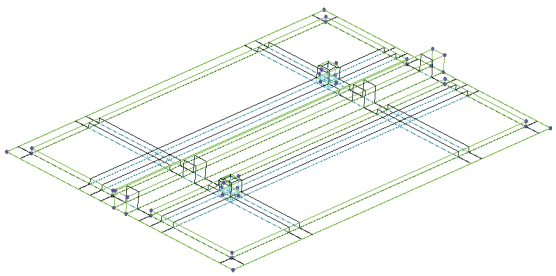

Fig. 4 Micro-clearance oil film grid model block map

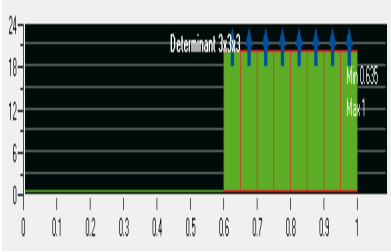

Fig. 5 Grid quality by 3x3x3

3.3 Boundary conditions

The boundary conditions used for the solution of temperature fields are as follows: the pressure on the external boundary is 0 MPa, the pressure for nodes on the pocket boundary is the same, the flow of lubricant through the hole is equal to the bearing input flow, the temperature of lubricant is the temperature of the surrounding atmosphere on the external boundary, the temperature of lubricant through the hole is the temperature of the oil chamber. The boundary conditions of the oil film are shown in Fig. 6.

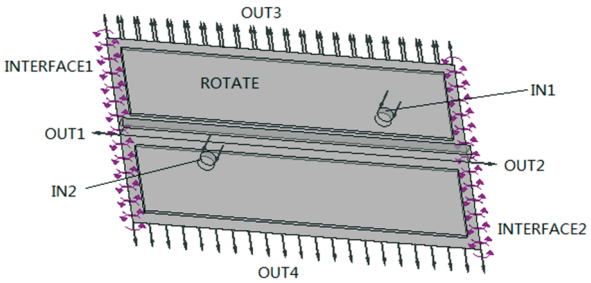

Fig. 6 Boundary conditions

3.4 Calculation accuracy control

The calculation model of the fluid is the total energy dissipation model which takes into account the effects of fluid kinetic energy. The convergence of the iteration residual curve is less than 10^{-4}, which can be used for post-processing calculation, and the number of iterations to solve the operation is 100. The iteration residual curve is shown in Figure 7.

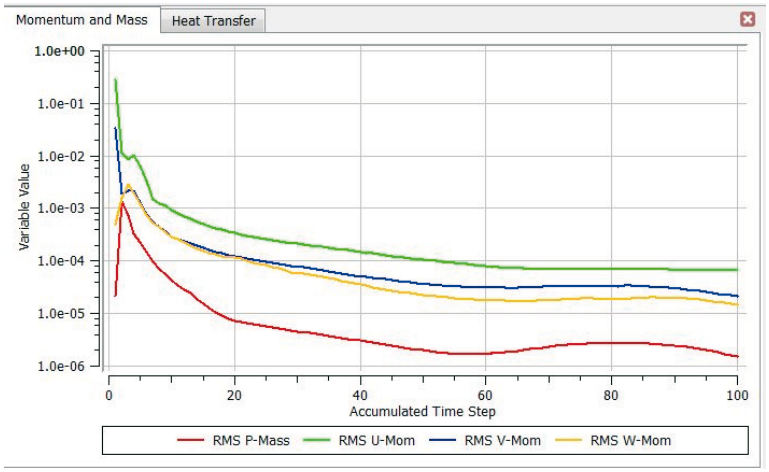

Fig. 7 Iteration residual curve

4. Results and discussion

The parameters of the lubricant used in the numerical simulation are the same as those of the ISO 32 lubricant tested in the factory. The density is 872 kg/m^3, the specific heat capacity is 1884 J/kg·K, the thermal conductivity is 0.132 W/m·K, the dynamic viscosity is 0.3365 p_a·s, the coefficient of thermal expansion is 0.00087 K^{-1}, and the ambient temperature is 15 °C. The temperature fields of oil film under different extreme operating conditions are simulated; the extreme operating conditions include 0t-228.9r/min, 8t-196.7r/min, 16t-162.4r/min, 24t-127.1r/min, and 32t-78.9r/min. The oil film temperature fields are shown in Figures 8 to 12.

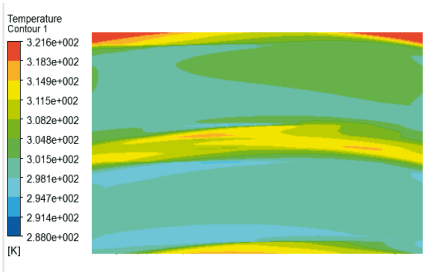

Fig. 8 Oil film temperature field with 0t-228.9r/min

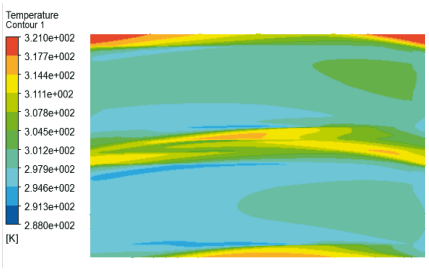

Fig. 9 Oil film temperature field with 8t-196.7r/min

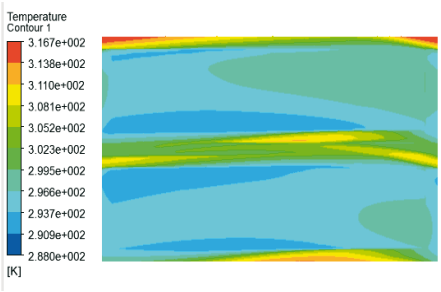

Fig. 10 Oil film temperature field with 16t-162.4r/min

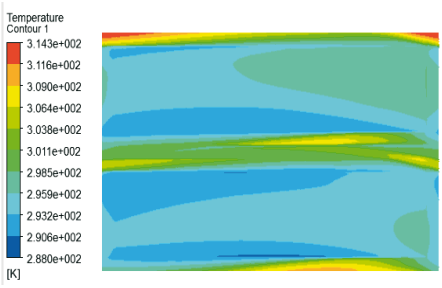

Fig. 11 Oil film temperature field with 24t-121.1r/min

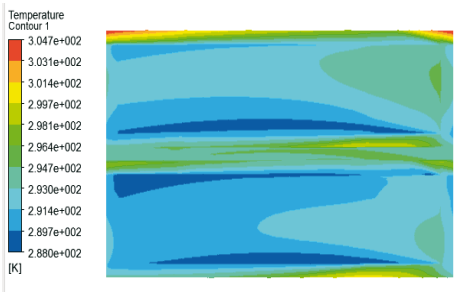

Fig. 12 Oil film temperature field with 32t-78.9r/min

From Figures 8 to 12 one can see that the temperature distribution of the micro-clearance oil film is roughly the same, and the temperature field of the oil film is unevenly distributed. The highest temperature is distributed on the outer side of the oil sealing edge, while the temperature of the oil film on the inner side of the oil sealing edge is in the middle; the temperature rise on the upstream side is sharper than that of the downstream side. It is mainly due to the combined influence of rotational linear velocity, dynamic pressure, and flow. The maximum and the average temperature of the oil film under different loads are shown in Fig. 13.

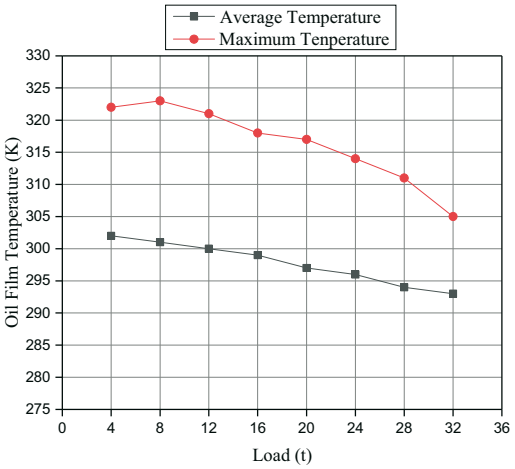

Fig. 13 Variation in the oil film temperature under different loads

It can be found from Figure 13 and Table 1 that both the rotational speed and the load have an influence on the temperature rise of the oil film, but the influence of the rotational speed on the temperature rise of the oil film is greater than that of the load.

5. Experiment on temperature field characteristics

The experiment was carried out on a heavy-duty CNC lathe of Qiqihar Heavy CNC Equipment Corp. LTD. Five JWB integrated temperature sensors were used to test the temperature field of micro-clearance oil film under different extreme conditions. The structure of oil pad on the base is shown in Fig. 14, the installation position of the temperature sensor is shown in Fig. 15, and the data display setup is shown in Fig. 16.

Fig. 14 Test rig

Fig. 15 Temperature sensors

Fig. 16 Data display setup

The temperature rise under loads of 0t and 12t was tested respectively, while the rotational speed of the turntable gradually increased from 0r/min with an increment of 20 r/min. Based on the experimental data, the relationship between rotational speed and temperature rise are shown in Fig. 17 and Fig. 18.

Fig. 17 Relationship between temperature rise and rotational speed at different positions under 0t

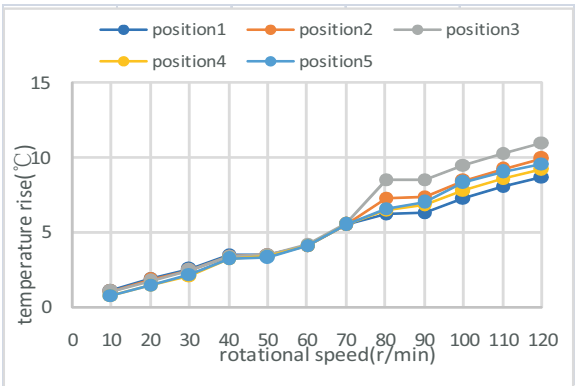

Fig. 18 Relationship between temperature rise and rotational speed at different positions under 12t

It can be seen from Fig. 18 that the larger the oil chamber load is at the same rotational speed, the faster the oil film temperature rises. When the load is constant, the temperature rise continues to increase with the increase in rotational speed. The results show that both the rotational speed and the load have an effect on the temperature rise. By comparing the data in Fig. 17 and Fig. 18, one can see that when the rotational speed increases to a certain extent, the slope of the temperature rise increases. Therefore, it can be concluded that the influence of rotational speed on the oil film temperature rise is greater than that of load. The temperature rise of the oil film at different positions is different; the temperature rise in the positions of sensors 3 and 5 is the highest, and the temperature rise in the positions of sensors 1 and 4 is relatively low. The sensor 1 is located inside the inner oil chamber. At the same speed, the linear velocity of the sensor 1 is the smallest, and the oil film shear force generates less heat per a unit of time, so the temperature in the position of the sensor 1 rises slowly. The sensor 4 is located on the downstream side of the oil chamber; the flow on the downstream side is large, and the amount of heat taken away by the lubricating oil is large, so the temperature rise in the position of sensor 4 is low. The sensor 5 is located on the upstream side of the oil chamber, and the upstream side flow is large; the heat is carried by the hot lubricating oil, so the temperature rise in the position of sensor 5 is high.

6. Conclusions

The relationship between the rotational speed and the load of the hydrostatic turntable under extreme operating conditions is deduced, and the inertia flow rate of the double rectangular chamber is calculated according to the principle of computational fluid dynamics. A 3D physical model of micro-clearance oil film is established and solved using the finite volume method. The micro-clearance oil film temperature field is also investigated and tested. When the extreme operating conditions are between 0t-228.9 r/min and 4t-214.9 r/min, the maximum temperature of the oil film rises slowly, while the average temperature decreases slowly. When the extreme operating conditions are between 4t-214.9 r/min and 32t-78.9 r/min, the maximum temperature and the average temperature showed a tendency to decrease slowly. Through the analysis of temperature rise data, it can be concluded that both the load and the rotational speed have an effect on the temperature rise. However, under extreme operating conditions, the effect of rotational speed on temperature is stronger than that of load. The temperature on the upstream side rises more sharply than that on the downstream side; also, the temperature on the outside of the oil chamber rises more sharply than that of the inside of the oil chamber and is nonlinear. The research results provide a theoretical basis for the temperature

control of the oil film in the clearance of the hydrostatic thrust bearing, the adjustment of the oil film stiffness, the research on the deformation of the bearing friction pair, and the stability of the hydrostatic bearing system.

Acknowledgement

The financial support for this study was provided by the National Key Research and Development Project (2022YFB3404902).

REFERENCES

[1] Heng F Q. *Analysis and optimization of the thermal characteristics of heavy-duty cnc vertical hydrostatic turntable*. Dissertation of University of electronic science and technology, Chengdu, China,**2015**.

[2] Zhang Y Q. Temperature field and experiment of hydrostatic bearing oil film based on hot oil carrying. *Journal of Jilin university (Engineering and Technology Edition)*, **2019**, 49(4): pp. 1203-1211.

[3] Zhang Y Q. Heavy load characteristics of micro-beveled heavy-duty hydrostatic bearing lubricant oil film. *PROCEEDINGS OF THE INSTITUTION OF MECHANICAL ENGINEERS PART J-JOURNAL OF ENGINEERING TRIBOLOGY*, **2020**, 235(4): pp. 738-747. https://doi.org/10.1177/1350650120920498

[4] Zhang Y Q. Temperature rise characteristics of beveled oil pad hydrostatic bearing under the influence of hot oil carrying. *Journal of Huazhong University of Science and Technology (Natural Science Edition)*, **2020**, 48(7): pp. 122-127.

[5] Zhang Y Q. High-speed characteristics of micro-beveled heavy duty hydrostatic bearing lubricant oil film. *Journal of Jilin University (Engineering and Technology Edition)*, **2021**, 51(2): pp. 450-457.

[6] Yu X D, Fu X, etc. The hydrostatic thrust bearing of the ring cavity is hot deformation. *Journal of Jilin university (engineering edition)*, **2015**, 45(2): pp. 460-465.

[7] Yu X D, Sun D D, Wu X G, Sui J L, Liu D, Fu X. High speed and heavy load characteristic on oil film thickness of annular thrust multi-pad hydrostatic bearing. propulsion technology, **2016**, 37(7): pp.1350-1355.

[8] Fathimunnisa Begum. Tribological experimentations with jatropha biofluid and nanoparticles as lubricant additives. *Transactions of FAMENA*, **2022**, 46(3): pp.41-50. https://doi.org/10.21278/TOF.463024920

[9] Ma T, Dai H L, Liu S E . Numerical simulation of liquid hydrostatic bearing based on FLUENT. *Journal of Donghua university (Natural science)*, **2010**, 36(6): pp.39-42.

[10] Wang J Y. Simulation and analysis of the heating performance of an embossing-head utilizing electromagnetic induction heating. *Transactions of FAMENA*, **2021**, 45(3): pp.101-113. https://doi.org/10.21278/TOF.453009319

[11] Zhang J D. Numerical simulation analysis of flow field for oil film of hydrostatic rotary worktable. *Journal of Machine Design*, **2019**, 36 S2: pp.104-108.

[12] Nikola Vujnović. Differences in calculations of annual heating and cooling energy need carried out by modified simple hourly method and dynamic simulations. *Transactions of FAMENA*, **2021**, 45(SI-1): pp.35-48. https://doi.org/10.21278/TOF.SI1007021

[13] Fang L, Chen G D. Flow and temperature characteristics of wall film in bearing chamber located in hot region of aero-engine. *Journal of aerospace Power*, **2020**,35(4): pp.682-692.

[14] Šefik Behrem. Results of heat transfer coefficient estimation during the quenching of cylindrical samples in aqueous solutions. *Transactions of FAMENA*, **2021**, 45(SI-1): pp.49-58. https://doi.org/10.21278/TOF.SI1008421

[15] Shao J P, Zhang Y Q, Yu X D. Numerical simulation and analysis of the temperature field in the fan cavity and circular cavity of heavy hydrostatic bearing. *Hydrodynamics research and progress*, **2009**,24(1): pp.119-124.

[16] Lang J, Yang J G, Cao H. Thermal effect analysis of sliding bearing and reasonable determination of equivalent temperature of flow field. *Lubrication Engineering*, **2012**, 37(10): pp.70-73.

[17] Liu D Q, Miao T C. Study on the steady heat effect of one-dimensional temperature field of sliding bearing. *Journal of Chinese electrical engineering*, **2010**, 30(32): pp.29-32.

[18] Zhang G T. Temperature distribution and heat generating/transfer mechanism of the circular bilayer porous bearing for thermo-hydrodynamic problem. *International Journal of Heat and Mass Transfer*, **2019**, 149. https://doi.org/10.1016/j.ijheatmasstransfer.2019.119134

[19] Brito F P, Miranda A S. Experimental investigation of the influence of supply temperature and supply pressure on the performance of a two axial groove hydrodynamic journal bearing. *ASME Journal of Tribology*, **2007**, 129(1): pp.98-105. https://doi.org/10.1115/1.2401206

[20] Singh U, Roy L, Sahu M (2008). Steady-state thermo-hydrodynamic analysis of cylindrical fluid film journal bearing with an axial groove. *Tribology International*, **2008**, 41(2): pp.1135-1144. https://doi.org/10.1016/j.triboint.2008.02.009

[21] Ding Zhenqian. Designs of the liquid hydrostatic. *Supporting. Shanghai: Shanghai science and technologypress.***1986**.

[22] Chen Yansheng. Designs and principle of the liquid hydrostatic supporting. *Beijing: National defence industry press*. **1980**.

[23] F.M. Adam Stansfield. Application of hydrostatic bearing in machine tools. *Beijing: China Machine Press.***2003**.

[24] Chen B X. Fluid lubrication theory and its application. *Beijing: Mechanical industry press.* **1991**: pp.30-60.

[25] Zhang B Z. Numerical methods of fluid dynamics. *Beijing: China Machine Press.***2003**.

[26] Wang F J. Calculation flow mechanics analyses FLUENT software principle and applies. *Beijing: TsingHua University press*. **2004**.

[27] Han Z Z, Wang J, Lan X P. The FLUENT fluid project simulates calculating an example and applies, *Beijing: Press of Beijing institute of technology*. **2004**.

Submitted: 14.5.2021

Accepted: 22.12.2022

Xiaodong Yu*
Zelin Han
Shiwei Zhan
Defan Zhou
Fakun Wang
Fan Sun
Key Laboratory of Advanced Manufacturing and Intelligent Technology, Ministry of Education, Harbin University of Science and Technology, Harbin 150080, China
Jianhua Jiao
Junfeng Wang
Hui Jiang
Qiqihar Heavy CNC Equipment Corp. LTD., Qiqihar 161005, China
*Corresponding author:
yuxiaodong@hrbust.edu.cn